ChemPubSoc Europe

DOI: 10.1002/chem.201402466

CHEMISTRY
A European Journal
Communication

Liquid Crystals

Thermotropic Luminescent Clustomesogen Showing a Nematic Phase: A Combination of Experimental and Molecular Simulation Studies

Maria Amela Cortes,[a] Frederick Dorson,[a] Marianne Prévôt,[a] Aziz Ghoufi,*[b] Bruno Fontaine,[a] Florent Goujon,[c] Régis Gautier,[a] Viorel Cîrcu,[d] Cristelle Mériadec,[b] Franck Artzner,[b] Hervé Folliot,[e] Stéphane Cordier,[a] and Yann Molard*[a]

Abstract: Octahedral Mo_6 nanoclusters are functionalized with two organic ligands containing cyanobiphenyl (CB) units, giving luminescent hybrid liquid crystals (LC). Although the mesogenic density around the bulky inorganic core is constant, the two hybrids show different LC properties. Interestingly, one of them shows a nematic phase, which is particularly rare for this kind of supermolecular system. This surprising result is explained by using large-scale molecular dynamic simulations.

Molybdenum is a low cost versatile transition metal that is used for many industrial applications, such as in alloy reinforcement, lubrication, and nuclear energy. It was also one of the principal constituents of filament supports in incandescent lamps or of filaments in electrical devices. However, since the production of light bulbs has stopped because of their high energy cost and their low efficiency compared with LED technology, new prospects should be found for this element, keeping in mind that industry needs low cost processes generating low cost materials. The use of supramolecular chemistry concepts, such as molecular self-assembly, which mainly issue from the world of organic and coordination molecular chemistry, is a promising way to generate new materials organized at the molecular scale. These materials are usually obtained with an all-organic approach, but recently, the field of hybrid materials has emerged and represents an outstanding alternative to generate low cost materials with increased functionalities.[1] Indeed, by using this powerful approach, one can design nanostructured self-organized hybrid functional materials where the functionality is given by nanometer-sized inorganic moieties whereas the self-organization is predominantly directed by their organic counterparts. Octahedral molybdenum nanoclusters, obtained by high temperature solid-state synthesis,[2] are interesting functional building blocks for the design of such hybrid materials. The full delocalization of their metallic electrons around the metallic scaffold induces unique intrinsic properties such as phosphorescence in the red–near IR area with large Stokes shifts, high quantum yields, long lived excited states on the order of the several tens of microseconds, electrogenerated luminescence, redox properties, and photocatalytic activity.[3] Taking into account the high price and the rarity of rare-earth metals usually used in display or lighting applications, and comparing these parameters to the efficiency of Mo_6 clusters, the latter should play a major role in the future in the luminescent dye category with applications in light, display, solar cell, detectors, and biological sensing technologies. However, the major drawback of Mo_6 clusters is their ceramic-like behavior in the solid state, which precludes their integration "right from the oven" in easy-to-shape materials and, as a result, adopting a hybrid strategy seems to be one of the most promising way to overcome this.[4] Thus, metallic clusters have been modified with organic moieties leading to hexasubstituted hybrids where the organic ligands are orthogonally arranged around the cluster core.[2b,5] It is however challenging to obtain liquid crystalline octahedral metallic cluster complexes because the coordination behavior of the cluster is poorly compatible with the structural requirements of liquid crystal phases (disk-like or rod-like geometry).[6] Nevertheless, we recently demonstrated the feasibility of the incorporation of such clusters into a liquid crystal (LC) matrix by substitution of their halogen apical ligands with promesogenic units[7] or by using specifically designed organic cations.[8] According to Saez and Goodby,[9] hexasubstituted clusters could be seen as monodispersed polypedal supermolecular materials in which

[a] Dr. M. A. Cortes, F. Dorson, M. Prévôt, Dr. B. Fontaine, Prof. R. Gautier, Dr. S. Cordier, Dr. Y. Molard
Université de Rennes 1 – ENSC Rennes – CNRS UMR 6226 "Institut des Sciences Chimiques de Rennes"
Campus de Beaulieu, CS 74205, 35042 Rennes Cedex (France)
E-mail: yann.molard@univ-rennes1.fr

[b] Dr. A. Ghoufi, C. Mériadec, Dr. F. Artzner
Université de Rennes 1, UMR Institut de Physique de Rennes
UR1-CNRS 6626, Campus de Beaulieu
CS 74205, 35042 Rennes Cedex (France)
E-mail: aziz.ghoufi@univ-rennes1.fr

[c] Dr. F. Goujon
ICCF – Institut de Chimie de Clermont-Ferrand
Equipe "Thermodynamique et Interactions Moléculaires"
UMR CNRS 6296/Université Blaise Pascal
24, avenue des Landais, 63177 Aubiere Cedex (France)

[d] Dr. V. Cîrcu
Department of Inorganic Chemistry, University of Bucharest
Dumbrava Rosie 33, Bucharest 020464, sector 2 (Romania)

[e] Prof. H. Folliot
Université Européenne de Bretagne, INSA Rennes, France and CNRS
UMR 6082 Foton, 20 Avenue des Buttes de Coësmes, 35708 Rennes (France)

Supporting information for this article is available on the WWW under http://dx.doi.org/10.1002/chem.201402466.

the metallic cluster plays the role of the central hard core scaffold in the dendritic architecture, with mesogenic units attached at terminal positions to this core by a spacer chain. In such a case, layered LC phases (SmA and SmC) are usually observed.[9–10] We report here two cyanobiphenyl (CB)-containing clustomesogens, one of which constitutes a very rare example of nematogenic ionic compound.[11]

The strategy used to obtain LC hybrid clusters is based on the grafting of mesomorphic promoters through a flexible aliphatic spacer onto the bulky isotropic inorganic moiety by reaction, in our case, of benzoic acid derivatives with $(n\mathrm{Bu_4N})_2[Mo_6Br_8F_6]$ as previously described.[7] These carboxylic acid derivatives, namely $HL^{3,4}$ and $HL^{3,5}$, are isomers and are based on a disubstituted benzoic acid scaffold linked to two CB moieties by an alkyl chain containing ten carbon atoms (Scheme 1). They were obtained in three steps according to reported procedures for similar compounds.[12] They were chosen for this

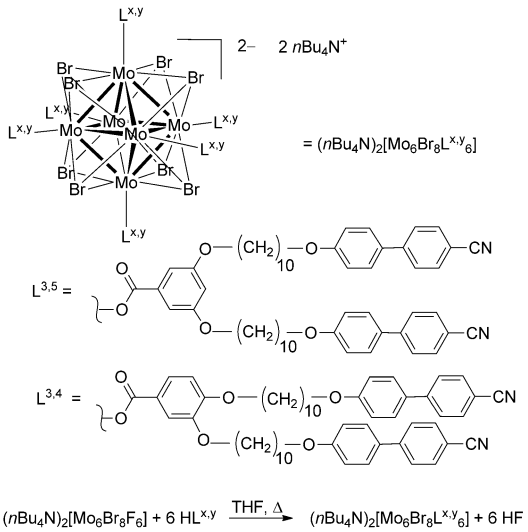

Scheme 1. Representation of $(n\mathrm{Bu_4N})_2\ [Mo_6Br_8L^{x,y}_6]$.

study as they are compounds for which the mesogenic density is reduced by 1/3 compared with previously reported results, and also to observe the influence of the benzoic scaffold substituent position on the liquid crystal properties of the resulting hybrid. The grafting reaction was confirmed by IR spectroscopy, ^{1}H NMR spectroscopy, and elemental analysis.

The thermal and liquid crystal (LC) properties of $(n\mathrm{Bu_4N})_2[Mo_6Br_8L^{x,y}_6]$ were investigated by differential scanning calorimetry (DSC), polarized optical microscopy (POM), and small-angle X-Ray scattering (SAXS). The phase transition and thermodynamic data are reported in Table 1 together with computed values of the temperatures for the phase transitions. Even though both compounds possess the same mesogenic density around their central core, their mesomorphic behavior is different. The DSC thermogram of $(n\mathrm{Bu_4N})_2[Mo_6Br_8L^{3,5}_6]$ shows two broad peaks at 83 and 94 °C, on both heating and cooling, that were assigned, by combination with POM observations

Table 1. Phase behavior, transition temperatures, and melting enthalpies of $(n\mathrm{Bu_4N})_2[Mo_6Br_8L^{x,y}_6]$ taken from the second heating cycle.

Compound	Transition	T [°C]	T_{sim} [°C]	ΔC_p [kJ mol^{-1} K^{-1}]	ΔH [kJ mol^{-1}]	ΔH per CB unit [kJ mol^{-1}]
$(n\mathrm{Bu_4N})_2[Mo_6Br_8L^{3,5}_6]$	G→SmA	19	–	3.02	–	–
	SmA→N	83[a]	87	–	12.70[b]	1.1[b]
	N→I	94[a]	97	–	–	
$(n\mathrm{Bu_4N})_2[Mo_6Br_8L^{3,4}_6]$	G→SmA	19		4.27	–	–
	SmA→I	103	97		33.8	2.8

[a] These values represent the temperatures taken from microscopy. [b] Combined enthalpies.

(Figures S4 and S7), to the Smectic A (SmA)–nematic and nematic–isotropic (I) phase transitions, respectively. The enthalpy parameters associated with these two transitions could not be extracted owing to the difficult separation of the two transitions, which was not possible even when a lower heating rate (5 °C min^{-1}) was used to record the thermogram. Thus, only a combined enthalpy is reported in Table 1. On cooling the cluster below room temperature, a glass transition could be detected from the DSC curve at 19 °C. On cooling $(n\mathrm{Bu_4N})_2[Mo_6Br_8L^{3,4}_6]$ from its isotropic melt at 10 °C min^{-1}, a first-order transition at 103 °C was observed, followed by a second-order transition at 20 °C. These were attributed to the I–SmA and SmA–G phase transitions, respectively. For both compounds, all heating and cooling cycles were superimposeable, attesting about their thermal stability.

Temperature-dependent X-ray diffraction experiments were carried out on aligned (Figure 1 a) and non-aligned samples to confirm the nature of the obtained mesophases (Figure S8, see the Supporting Information). From 85 to 95 °C, the observation

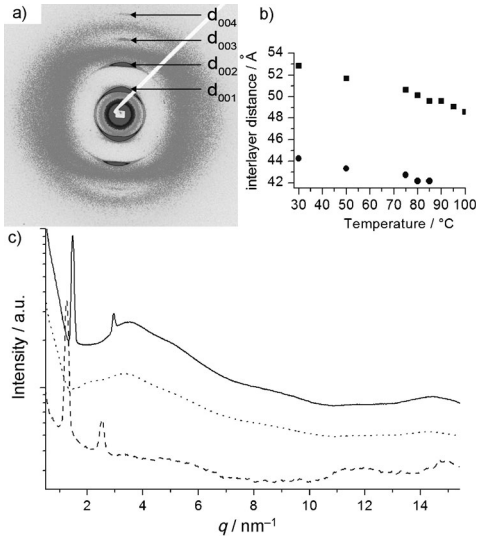

Figure 1. a) Two-dimensional X-ray diffraction pattern of $(n\mathrm{Bu_4N})_2[Mo_6Br_8L^{3,5}_6]$ obtained at 25 °C. b) Evolution of interlayer distances in the smectic phase versus temperature for $(n\mathrm{Bu_4N})_2[Mo_6Br_8L^{3,5}_6]$ (circles) and $(n\mathrm{Bu_4N})_2[Mo_6Br_8L^{3,4}_6]$ (squares). c) Integrated X-ray diffraction patterns of $(n\mathrm{Bu_4N})_2[Mo_6Br_8L^{3,5}_6]$ at 80 °C (solid line) and 90 °C (dotted line) and $(n\mathrm{Bu_4N})_2[Mo_6Br_8L^{3,4}_6]$ at 80 °C (dashed line).

of a broad and intense scattering signal in the small-angle region instead of the presence of sharp intense peaks confirmed the absence of 1D or 2D long-range correlated positional ordering for $(n\mathrm{Bu_4N})_2[\mathrm{Mo_6Br_8L_6^{3,5}}]$. These signals, the maxima of which are located at 3.3 and 2.3 $\mathrm{nm^{-1}}$, correspond to lateral short-range molecular correlations of the electron-rich cluster moieties and are typical of orientational nematic ordering. In the wide-angle part, a diffuse scattering halo at approximately 4.3 Å, attributed to the lateral short-range order of the molten chains and cyanobiphenyl moieties, confirms the liquid crystalline nature of the mesophase. Below 85 °C, two additional sharp small-angle reflections, characteristic of a layered morphology with a reciprocal spacing in the 1:2 ratio, are present in the X-ray diffraction patterns of both components. By applying Bragg's law to these maxima at, for example, 80 °C, layer spacing distances of 42.2 and 50.1 Å were calculated for $(n\mathrm{Bu_4N})_2[\mathrm{Mo_6Br_8L_6^{3,5}}]$ and $(n\mathrm{Bu_4N})_2[\mathrm{Mo_6Br_8L_6^{3,4}}]$, respectively. Lowering the temperature to 30 °C induces a slight increase in the interlayer spacing of about 2 Å. Additional very broad and intense reflections (maximum located around 3.7 $\mathrm{nm^{-1}}$) without any straightforward correlations are observed and are more pronounced for $(n\mathrm{Bu_4N})_2[\mathrm{Mo_6Br_8L_6^{3,5}}]$. These reflections reveal the absence of clear positional ordering within the electron-rich cluster layer. Thus, the observed patterns correspond to disordered smectic layers (SmA) and are consistent with the obtained POM textures. Therefore, both compounds are liquid crystalline at room temperature and, despite the same mesogenic density around the central metallic core, $(n\mathrm{Bu_4N})_2[\mathrm{Mo_6Br_8L_6^{3,5}}]$ shows a nematic phase and a smectic phase whereas $(n\mathrm{Bu_4N})_2[\mathrm{Mo_6Br_8L_6^{3,4}}]$ shows only a smectic phase with interlayer spacing always around 1 nm larger than that of $(n\mathrm{Bu_4N})_2[\mathrm{Mo_6Br_8L_6^{3,5}}]$ at the same temperature (Figure 1 b).

To explain the lack of nematic phase in $(n\mathrm{Bu_4N})_2[\mathrm{Mo_6Br_8L_6^{3,4}}]$ and the influence of the benzoate substituent position on the interlayer distance, large-scale molecular dynamic simulations (MD) were carried out (see the Supporting Information for computational details). The force field and computational procedures were validated by calculation of the translational (τ) and orientational (S) order parameters[13] related to smectic (Sm) and nematic (N) order. τ and S are reported with respect to the temperature for both compounds in Figure S10 (see the Supporting Information). For $(n\mathrm{Bu_4N})_2[\mathrm{Mo_6Br_8L_6^{3,5}}]$, the sudden increase in τ and S with decreasing temperature clearly shows that I→N and N→Sm transitions occur. Conversely, with $(n\mathrm{Bu_4N})_2[\mathrm{Mo_6Br_8L_6^{3,4}}]$ the nematic phase is not present. This result is in good agreement with experiments and validates the present computational protocol and force field. To understand the absence of the nematic phase for $(n\mathrm{Bu_4N})_2[\mathrm{Mo_6Br_8L_6^{3,4}}]$, the structural conformation of both components in the isotropic phase (at 420 K) was investigated from their asphericity (A_s) and their radius of gyration (R_g) by looking at their components according to the x, y, and z directions. The radii of gyration in the z-direction (R_{gz}) for $(n\mathrm{Bu_4N})_2[\mathrm{Mo_6Br_8L_6^{x,y}}]$ are reported in Figure 2 a and b. $(n\mathrm{Bu_4N})_2[\mathrm{Mo_6Br_8L_6^{3,4}}]$ seems to be more elongated than $(n\mathrm{Bu_4N})_2[\mathrm{Mo_6Br_8L_6^{3,5}}]$. Indeed, a difference of about 10 Å was found. This is borne out by the calculation of A_s. For $(n\mathrm{Bu_4N})_2[\mathrm{Mo_6Br_8L_6^{3,5}}]$ A_s is 0.4 whereas for $(n\mathrm{Bu_4N})_2[\mathrm{Mo_6Br_8L_6^{3,4}}]$ A_s is 0.08. These values indicate a preferential cylindrical conformation for $(n\mathrm{Bu_4N})_2[\mathrm{Mo_6Br_8L_6^{3,4}}]$ and a structure with a larger base for $(n\mathrm{Bu_4N})_2[\mathrm{Mo_6Br_8L_6^{3,5}}]$. This elongation is confirmed by the gyration's radii in the x and y directions as we found $R_{gx}((n\mathrm{Bu_4N})_2[\mathrm{Mo_6Br_8L_6^{3,5}}]) > R_{gx}((n\mathrm{Bu_4N})_2[\mathrm{Mo_6Br_8L_6^{3,4}}])$. This result is in accordance with the difference in interlayer spacing calculated from the SAXS experiments (around 1 nm). Thus, both compounds keep a global cylindrical geometry and the absence of a nematic phase for $(n\mathrm{Bu_4N})_2[\mathrm{Mo_6Br_8L_6^{3,4}}]$ is obviously unconnected to the geometrical form of the supermolecular system. Therefore, another physical component must be found to explain this behavior. From an energetic standpoint, in the isotropic phase of $(n\mathrm{Bu_4N})_2[\mathrm{Mo_6Br_8L_6^{3,4}}]$, the intermolecular interactions are sufficiently favorable to avoid a transition to nematic organization when the temperature decreases. Indeed, this decrease acts as a thermal stimulus and allows a new minimum of interactions to be reached, inducing a phase transition. The ranges in which the isotropic, nematic, and smectic phases exist generally overlap; however, the smectic phase is the most stable and has the lowest free energy thanks to combined propagation of the orientational and translational orders (Figure S10). The structural situation differs in the case of $(n\mathrm{Bu_4N})_2[\mathrm{Mo_6Br_8L_6^{3,5}}]$. Indeed, as a nematic phase is observed around 370 K, $(n\mathrm{Bu_4N})_2[\mathrm{Mo_6Br_8L_6^{3,5}}]$ self-organizes such that the nematic domain is energetically favorable. As depicted in Figure 2, the conformation of the minimized structure of $(n\mathrm{Bu_4N})_2[\mathrm{Mo_6Br_8L_6^{3,5}}]$ suggests full interdigitation between the cyanobiphenyl groups (CB) of adjacent layers. Indeed, taking into account an average cross-section of 24 $\mathrm{Å^2}$ per CB (the usual value lays between 22–25 $\mathrm{Å^2}$),[7] full interdigitation of 12

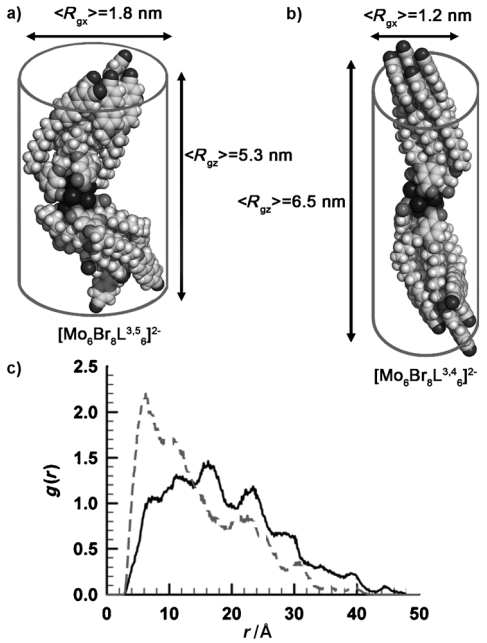

Figure 2. Representation of a) $[\mathrm{Mo_6Br_8L_6^{3,5}}]^{2-}$ and b) $[\mathrm{Mo_6Br_8L_6^{3,4}}]^{2-}$ according to molecular modelling experiments. c) Distribution of d_{NN} for $[\mathrm{Mo_6Br_8L_6^{3,5}}]^{2-}$ (solid line) and $[\mathrm{Mo_6Br_8L_6^{3,4}}]^{2-}$ (dashed line).

CB groups leads to a surface of 290 Å^2 (19.2 Å diameter), whereas the reverse situation gives a disc surface with a diameter of 13.5 Å. Both values are consistent with the average gyration radii calculated in the *x* direction.

This ability to interdigitate can also be evaluated from the calculation of d_{NN}, representing the distance between the terminal nitrogen atoms of two CB groups belonging to the same ligand, L; the distribution of d_{NN} is plotted in Figure 2c for both compounds (see Figure S11 in the Supporting Information for a graphical representation of the interdigitation). For $(n\mathrm{Bu_4N})_2[\mathrm{Mo_6Br_8L_6^{3,4}}]$, this distribution presents a maximum around 6 Å, whereas a broad distribution is observed with $(n\mathrm{Bu_4N})_2[\mathrm{Mo_6Br_8L_6^{3,5}}]$. This broadening clearly suggests that distances between 10 and 25 Å are sampled with the same probability. As it is well known that the lateral periodicity of CB in lamellar phases is about 4.5 Å, the minimum value of d_{NN} at which interdigitation can occur is around 9 Å. Thus, the $(n\mathrm{Bu_4N})_2[\mathrm{Mo_6Br_8L_6^{3,5}}]$ conformation allows the interdigitation process that leads to an increase in free energy and then to a transition toward a more stable nematic phase. In other words, the interdigitation "destabilizes" to generate nematic fluctuations. Conversely, the absence of entanglement in $(n\mathrm{Bu_4N})_2[\mathrm{Mo_6Br_8L_6^{3,4}}]$ prevents the isotropic destabilization and the nematic interactions. In this temperature range, the smectic fluctuations are favored, leading to the formation of the more stable Sm phase.

Despite the possibility to align $(n\mathrm{Bu_4N})_2[\mathrm{Mo_6Br_8L_6^{3,5}}]$ in its nematic phase by application of a magnetic field,[14] both hybrids remain very viscous and cannot be used directly in LC devices in which the molecular orientation is driven by an external stimulus. A possibility to increase their fluidity, and therefore demonstrate their potential for the building of such devices, is to combine them with commercially available highly fluidic liquid crystals with the prerequisite that resulting mixtures must be fully homogeneous. Figure 3 presents the POM pictures taken under white light and UV irradiation (λ_{exc} = 400 nm) for mixtures of $(n\mathrm{Bu_4N})_2[\mathrm{Mo_6Br_8L_6^{3,5}}]$ (a and b) and $(n\mathrm{Bu_4N})_2[\mathrm{Mo_6Br_8L_6^{3,4}}]$ (c and d) at 10 wt% in E44 LC (Merck). UV irradiation of both mixtures induces the typical luminescence of the clusters in the red–NIR area and reveals the repartition of the hybrid in the host matrix (see Figures S12–S14 in the Supporting Information for luminescence spectra of pure compounds at different temperatures and as mixtures in E44). Our attempts to observe polarized emission remained unsuccessful, which may be due to the isotropy of the emissive inorganic species.

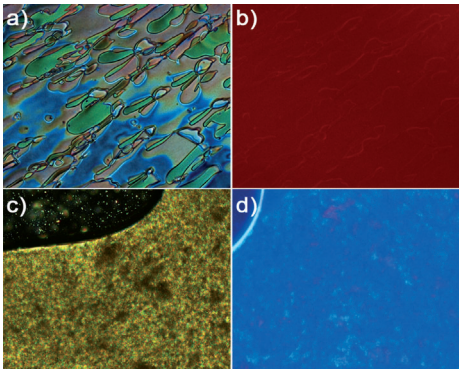

Figure 3. Polarized optical micrographs of a,b) E44/$(n\mathrm{Bu_4N})_2[\mathrm{Mo_6Br_8L_6^{3,5}}]$ (9:1) mixtures under white light (a) and UV irradiation (b, λ_{exc} = 400 nm), and c,d) E44/$(n\mathrm{Bu_4N})_2[\mathrm{Mo_6Br_8L_6^{3,4}}]$ (9:1) mixtures under white light (c) and UV irradiation (d, λ_{exc} = 400 nm).

As illustrated in Figure 3b and d, $(n\mathrm{Bu_4N})_2[\mathrm{Mo_6Br_8L_6^{3,5}}]$, which shows a nematic phase, is fully miscible with the nematogenic E44 (see Figure S15 in the Supporting Information for the DSC thermogram of $(n\mathrm{Bu_4N})_2[\mathrm{Mo_6Br_8L_6^{3,5}}]$ at 10 wt% in E44); however, $(n\mathrm{Bu_4N})_2[\mathrm{Mo_6Br_8L_6^{3,4}}]$, showing only a smectic phase, is not miscible. As the emissive excited state of transition-metal clusters is mainly metal centered,[15] the coordination of the promesogenic ligand onto the cluster induces no significant change in the emission properties of the cluster core (note that for Mo_6 clusters, Φ_{PL} values up to 0.80 have been recently reported[3d], Figure S12). This point is of significance because it shows that other ligands can be used to modify the LC properties of the hybrid material without altering its luminescence properties. Yet, it gives clustomesogens a major advantage over luminescent metallomesogens containing d-block elements for which most of the emissive excited states are not metal centered and thus the emission is strongly affected by the nature of the ligands and the intramolecular interactions in the mesophase.[16]

In conclusion, we synthesized new clustomesogens that show liquid crystalline properties at room temperature as well as red–NIR luminescence. In addition, the clearing point is observable around 100 °C, which makes this material suitable for processing of thin films by thermal annealing considering that the upper temperature limit for fabrication of devices on flexible plastic substrates is considered to be 200 °C.[17] The formation of a nematic phase for $(n\mathrm{Bu_4N})_2[\mathrm{Mo_6Br_8L_6^{3,5}}]$, the most fluidic of the liquid crystal phases, between 94 °C and 83 °C, allows the alignment of the molecules upon application of a magnetic field. The innovative approach of using a specific molecular modeling method that is usually used for inert compounds reveals that the presence of the nematic phase can be attributed to the ability of $(n\mathrm{Bu_4N})_2[\mathrm{Mo_6Br_8L_6^{3,5}}]$ to interdigitate with its neighbors. The fluidity of $(n\mathrm{Bu_4N})_2[\mathrm{Mo_6Br_8L_6^{3,5}}]$ can be significantly increased by mixing with commercially available LC mixtures such as E44. This miscibility, combined to the ease of synthesis of this class of compounds, makes them good candidates for further integration into devices such as flexible displays, solar cell concentrators, or sensors.

Acknowledgements

We are grateful to UR1, Fondation Langlois, and Region Bretagne (CREATE program) for financial support. This work has been performed in the frame of the PHC Brancusi Program No. 19616UF and ANR Clustomesogen ANR-13-BS07-0003-01.

Keywords: cluster compounds · hybrid materials · luminescence · molecular dynamics · self-assembly

[1] a) C. Sanchez, P. Belleville, M. Popall, L. Nicole, *Chem. Soc. Rev.* **2011**, *40*, 696; b) H. K. Bisoyi, S. Kumar, *Chem. Soc. Rev.* **2011**, *40*, 306.
[2] a) F. A. Cotton, *Inorg. Chem.* **1964**, *3*, 1217; b) S. Cordier, K. Kirakci, D. Mery, C. Perrin, D. Astruc, *Inorg. Chim. Acta* **2006**, *359*, 1705.
[3] a) A. W. Maverick, J. S. Najdzionek, D. MacKenzie, D. G. Nocera, H. B. Gray, *J. Am. Chem. Soc.* **1983**, *105*, 1878; b) A. W. Maverick, H. B. Gray, *J. Am. Chem. Soc.* **1981**, *103*, 1298; c) M. N. Sokolov, M. A. Mihailov, E. V. Peresypkina, K. A. Brylev, N. Kitamura, V. P. Fedin, *Dalton Trans.* **2011**, *40*, 6375; d) Y. Zhao, R. R. Lunt, *Adv. Energy Mater.* **2013**, *3*, 1143; e) A. Barras, S. Cordier, R. Boukherroub, *Appl. Catal. B* **2012**, *123 – 124*, 1; f) A. Barras, M. R. Das, R. R. Devarapalli, M. V. Shelke, S. Cordier, S. Szunerits, R. Boukherroub, *Appl. Catal. B* **2013**, *130 – 131*, 270.
[4] a) M. Amela-Cortes, A. Garreau, S. Cordier, E. Faulques, J.-L. Duvail, Y. Molard, *J. Mater. Chem. C* **2014**, *2*, 1545; b) Y. Molard, C. Labbe, J. Cardin, S. Cordier, *Adv. Funct. Mater.* **2013**, *23*, 4821.
[5] a) D. Méry, L. Plault, S. Nlate, D. Astruc, S. Cordier, K. Kirakci, C. Perrin, *Z. Anorg. Allg. Chem.* **2005**, *631*, 2746; b) S. Ababou-Girard, S. Cordier, B. Fabre, Y. Molard, C. Perrin, *ChemPhysChem* **2007**, *8*, 2086; c) L. F. Szczepura, K. A. Ketcham, B. A. Ooro, J. A. Edwards, J. N. Templeton, D. L. Cedeno, A. J. Jircitano, *Inorg. Chem.* **2008**, *47*, 7271; d) G. Prabusankar, Y. Molard, S. Cordier, S. Golhen, Y. Le Gal, C. Perrin, L. Ouahab, S. Kahlal, J. F. Halet, *Eur. J. Inorg. Chem.* **2009**, 2153; e) Y. Molard, F. Dorson, K. A. Brylev, M. A. Shestopalov, Y. Le Gal, S. Cordier, Y. V. Mironov, N. Kitamura, C. Perrin, *Chem. Eur. J.* **2010**, *16*, 5613.
[6] a) D. W. Bruce, *Adv. Mater.* **1994**, *6*, 699; b) R. W. Date, E. F. Iglesias, K. E. Rowe, J. M. Elliott, D. W. Bruce, *Dalton Trans.* **2003**, 1914.
[7] Y. Molard, F. Dorson, V. Circu, T. Roisnel, F. Artzner, S. Cordier, *Angew. Chem.* **2010**, *122*, 3423; *Angew. Chem. Int. Ed.* **2010**, *49*, 3351.
[8] Y. Molard, A. Ledneva, M. Amela-Cortes, V. Circu, N. G. Naumov, C. Meriadec, F. Artzner, S. Cordier, *Chem. Mater.* **2011**, *23*, 5122.
[9] I. M. Saez, J. W. Goodby, *Struct. Bonding (Berlin)* **2008**, *128*, 1.
[10] E. Terazzi, G. Rogez, J.-L. Gallani, B. Donnio, *J. Am. Chem. Soc.* **2013**, *135*, 2708.
[11] a) D. W. Bruce, D. A. Dunmur, P. M. Maitlis, P. Styring, M. A. Esteruelas, L. A. Oro, M. B. Ros, J. L. Serrano, E. Sola, *Chem. Mater.* **1991**, *3*, 378; b) D. W. Bruce, D. A. Dunmur, P. M. Maitlis, P. Styring, M. A. Esteruelas, L. A. Oro, M. B. Ros, J. L. Serrano, E. Sola, *Chem. Mater.* **1989**, *1*, 479.
[12] a) P. H. J. Kouwer, G. H. Mehl, *Mol. Cryst. Liq. Cryst.* **2003**, *397*, 1; b) P. H. J. Kouwer, J. Pourzand, G. H. Mehl, *Chem. Commun.* **2004**, 66.
[13] A. Ghoufi, G. Maurin, G. Ferey, *J. Phys. Chem. Lett.* **2010**, *1*, 2810.
[14] Due to its high viscosity, a 14 T magnetic field had to be employed to properly align $(n\mathrm{Bu_4N})_2[\mathrm{Mo_6Br_8L_6^{3,5}}]$ in the glass capillary used for SAXS measurements. The capillary was heated at 120 °C and cooled down to 20 °C in 4 h within the 14 T field.
[15] H. Honda, T. Noro, K. Tanaka, E. Miyoshi, *J. Chem. Phys.* **2001**, *114*, 10791.
[16] a) K. Binnemans, *J. Mater. Chem.* **2009**, *19*, 448; b) V. N. Kozhevnikov, B. Donnio, D. W. Bruce, *Angew. Chem.* **2008**, *120*, 6382; *Angew. Chem. Int. Ed.* **2008**, *47*, 6286.
[17] W. A. MacDonald, *J. Mater. Chem.* **2004**, *14*, 4.

Received: March 4, 2014
Published online on June 4, 2014